Layout Optimization of Unconstrained Viscoelastic Layer on Beams Using Fractional Derivative Model

D.-H. Lee*
Dongeui University, Busan 614-714, Republic of Korea
and
W.-S. Hwang†
Daegu University, Kyungbuk 712-714, Republic of Korea

Nomenclature

a_0, a_1, c_1, d_1, and β	=	material constants
b	=	design variable
E	=	storage modulus
$\boldsymbol{E}^*$	=	complex modulus
f	=	frequency
i	=	$\sqrt{-1}$
$[\boldsymbol{K}]$	=	global stiffness matrix
$[\boldsymbol{M}]$	=	global mass matrix
T	=	temperature
t	=	time
U	=	strain energy
$\{\boldsymbol{y}\}$	=	eigenvector
$\alpha(T)$	=	shift factor
δ_{ij}	=	Kronecker delta
ε	=	strain
η	=	loss factor
σ	=	stress
ς	=	eigenvalue ($= (2\pi f)^2$)

I. Introduction

THE amount of damping is the most important parameter in reducing the magnitude of response near resonance frequencies. In most cases, viscoelastic materials that have a high loss factor are added to structures in order to increase damping when resonance is inevitable. The dynamic properties of viscoelastic materials, such as the complex modulus and the loss factor, are highly nonlinear in terms of frequency and temperature. Many researchers have tried to optimize damping treatment configurations.[1,2] A few researchers have considered the nonlinearity of frequency, but these studies were not realistic, or a tabular form.[2]

In this research, the optimal configuration of unconstrained viscoelastic damping layer beams is obtained. The nonlinearity of viscoelastic materials is included in the optimization process using the four-parameter fractional derivative model in a finite beam element.

II. Analysis of Beam with Unconstrained Damping Layer

A. Fractional Derivative Model

The dynamic characteristics of viscoelastic materials in the frequency domain can be represented using a complex modulus such as

$$\bar{\sigma} = E^*\bar{\varepsilon} = E(1 + i\eta)\bar{\varepsilon} \tag{1}$$

where $\bar{}$ refers to the Fourier transform.

The complex modulus of the viscoelastic material is strongly dependent on temperature and frequency. From the temperature-frequency equivalence hypothesis,[3] any two complex moduli at different frequencies and temperatures have a relation such as

$$E^*(f_1, T_1) = E^*[f_2\alpha(T_2), T_2] \tag{2}$$

Therefore, by preparing a master curve at T_0 we can use the sift factor to predict the complex modulus at any given temperature. In addition, the shift factor and temperature can be related by the Arrhenius equation,[3] as in

$$\log[\alpha(T)] = d_1(1/T - 1/T_0) \tag{3}$$

where temperatures are in degrees absolute.

Assuming homogeneous isotropic materials and linearity with respect to vibration amplitudes, the constitutive equation of the fractional derivative model of order one[4] can be written as

$$\sigma(t) + c_1 D^\beta \sigma(t) = a_0\varepsilon(t) + a_1 D^\beta \varepsilon(t) \tag{4}$$

where $0 < \beta < 1$ and D^β indicate the fractional derivative.[4] The complex modulus of the fractional derivative model can be obtained by the Fourier transforms of Eq. (4) as follows:

$$\boldsymbol{E}^* = E(1 + i\eta) = \frac{a_0 + a_1[i f\alpha(T)]^\beta}{1 + c_1[i f\alpha(T)]^\beta} \tag{5}$$

In most cases, viscoelastic materials have one peak for the loss factor along frequencies. For the one-loss-peak materials, the four-parameter fractional derivative model[4] sufficiently represents the real behavior of viscoelastic materials over a wide frequency range.

B. Analysis of Beams with Unconstrained Viscoelastic Layer

Consider an unconstrained damping layer beam, as shown in Fig. 1. The equivalent complex flexural rigidity E^*I of the unconstrained beams by the Ross, Ungar, and Kerwin (RUK) equation[3] is written in the form

$$\frac{E^*I}{E_1^*I_1} = 1 + e^*h^3 + 3(1 + h)^3\frac{e^*h}{1 + e^*h} \tag{6}$$

where $h = H_2/H_1$ and $e^* = E_2^*/E_1^*$. The equivalent storage modulus and the loss factor of the unconstrained beam can be obtained from the real and imaginary parts of Eq. (6), respectively.

The unconstrained damping layer beams can be analyzed using a finite beam element formulation with equivalent flexural rigidity. For a partially covered unconstrained beam, as shown in Fig. 1, one can model the beam using finite beam elements with different stiffness values. By introducing a finite beam element, and ignoring shear deformations because the unconstrained beam undergoes primarily extensional bending, one can obtain the following eigenvalue problem:

$$[\boldsymbol{K}]\{\boldsymbol{y}\} = \varsigma[\boldsymbol{M}]\{\boldsymbol{y}\} \tag{7}$$

Here, the matrix $[\boldsymbol{K}]$ is a complex-valued matrix because the equivalent stiffness of the viscoelastic damping layer beam becomes a complex quantity. The eigenvalue problem of Eq. (7) is a nonlinear equation because the stiffness matrix is a function of frequency.

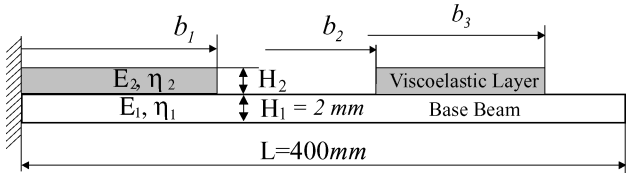

Fig. 1 Unconstrained damping layer beam and design variables.

Received 8 January 2004; revision received 22 June 2004; accepted for publication 22 June 2004; presented as Paper 2004-4419 at the AIAA/ISSMO 10th Multidisciplinary Analysis and Optimization Conference, Albany, NY, 30 August–1 September 2004.

*Assistant Professor, Department of Mechanical Engineering, 995 Eomgwangno, Busanjin-gu; dooho@deu.ac.kr. Member AIAA.

†Assistant Professor, School of Automotive, Industrial and Mechanical Engineering, Naeri, Kyungsan, Kyungbuk.

Therefore, an iteration procedure is necessary in order to solve the nonlinear eigenvalue problem.

The loss factor of a structure for the kth vibration mode[5] η^k is defined as

$$\eta^k = \sum_{j=1}^{p} \eta_j U_{ej} \Bigg/ \sum_{j=1}^{p} U_{ej} = \sum_{j=1}^{p} \eta_j U_{ej} \Bigg/ U \tag{8}$$

where p is the number of finite elements, η_j is a loss factor of the jth element, and $\boldsymbol{U}_{ej}$ is the strain energy of the jth finite element. To calculate the modal strain energy of the viscoelastic damping layer beam, one must first solve a complex eigenvalue problem. However, many researchers have shown that the real-eigenvector modal strain energy approach is in agreement with the complex-eigenvector modal strain energy approach.[5] Here, the real-eigenvector modal strain energy method is used to evaluate the loss factor of the unconstrained damping layer beam.

To validate the evaluation procedure of the system loss factor of unconstrained damping layer beams, a numerical example with a clamped-free boundary condition is introduced in Fig. 1. In the example, a viscoelastic damping material, LD-400, is bonded on an aluminum beam. Material properties used are listed in Table 1. The damping-treated beam is modeled with 20 beam elements for the case the coated length b_1 is 200 mm, and b_2 and b_3 are both zero. The analysis results are compared with those of MSC/NASTRAN using CQUAD4 and offset CBAR elements. Table 2 shows good agreement between the two methods in terms of the eigenfrequencies and the system loss factors, which proves that the proposed analysis procedure is accurate.

III. Design Sensitivity Analysis

To identify the optimal damping layout using gradient-based algorithms, a design sensitivity analysis for the loss factors is necessary. The design sensitivity data are obtained by differentiating the loss factor expression [Eq. (8)] with respect to the design variable as follows:

$$\frac{\mathrm{d}\eta^k}{\mathrm{d}b} = \left[\sum_{i=1}^{m} \left\{ \frac{\mathrm{d}\eta_i}{\mathrm{d}b} U_{ei} + \eta_i \frac{\mathrm{d}U_{ei}}{\mathrm{d}b} \right\} - \eta^k \frac{\mathrm{d}U}{\mathrm{d}b} \right] \Bigg/ U \tag{9}$$

For the unconstrained damping-layer-beam system, the element strain energy U_{ei} and the total strain energy U can be expressed, respectively, as

$$U_{ei} = \tfrac{1}{2}\{\boldsymbol{y}_i\}^T [\boldsymbol{K}_{ei}]\{\boldsymbol{y}_i\} \tag{10}$$

$$U = \tfrac{1}{2}\{\boldsymbol{y}\}^T [\boldsymbol{K}]\{\boldsymbol{y}\} \tag{11}$$

where $\{\boldsymbol{y}_i\}$ and $[\boldsymbol{K}_{ei}]$ are the eigenvector and the stiffness matrix of the ith element, respectively. To obtain the explicit expression $\mathrm{d}\eta_i/\mathrm{d}b$ of Eq. (9) can be rewritten using the chain rule as

$$\frac{\mathrm{d}\eta_i(b, f)}{\mathrm{d}b} = \frac{\partial \eta_i}{\partial b} + \frac{\partial \eta_i}{\partial f}\frac{\mathrm{d}f}{\mathrm{d}b} \tag{12}$$

The first term on the right-hand side of Eq. (12) can be evaluated analytically from Eqs. (5) and (6). In addition, the partial differentiation of the equivalent loss factor of the ith element for the viscoelastic damping layer beams is obtained from Eq. (6) as

$$\frac{\partial \eta_i}{\partial f} = \frac{\mathrm{Im}(\partial \boldsymbol{E}^*/\partial f) \cdot \mathrm{Re}(\boldsymbol{E}^*) - \mathrm{Im}(\boldsymbol{E}^*) \cdot \mathrm{Re}(\partial \boldsymbol{E}^*/\partial f)}{[\mathrm{Re}(\boldsymbol{E}^*)]^2} \tag{13}$$

where $\mathrm{Im}(\cdot)$ and $\mathrm{Re}(\cdot)$ are the imaginary and real parts of the argument, respectively. The partial derivative of the complex modulus with respect to frequency $\partial \boldsymbol{E}^*/\partial f$ in Eq. (13) can be derived analytically from Eqs. (5) and (6). Consequently, the right-hand side of Eq. (13) can also be calculated. Next, the frequency variation with respect to the design variable $\mathrm{d}f/\mathrm{d}b$ in Eq. (12) can be calculated by the eigenvalue sensitivity formula[6] for the ith eigenvalue:

$$\dot{\varsigma}^i = \{\boldsymbol{y}^i\}^T \left[\frac{\partial \boldsymbol{K}}{\partial b} \right] \{\boldsymbol{y}^i\} - \varsigma^i \{\boldsymbol{y}^i\}^T \left[\frac{\partial \boldsymbol{M}}{\partial b} \right] \{\boldsymbol{y}^i\} \tag{14}$$

Finally, the first term of the numerator of the loss factor sensitivity expression [Eq. (9)] can now be calculated.

Next, by combining the loss factor sensitivity Eq. (9) and the modal strain energy expressions in Eqs. (10) and (11), one can see that the second and the third terms of the numerator of the loss factor sensitivity formula can be expressed with $\partial \boldsymbol{K}/\partial b$ and eigenvector sensitivity $\{\partial \boldsymbol{y}^i/\partial b\}$ using the chain rule. The eigenvector sensitivity[7] can be written as

$$\left\{ \frac{\partial \boldsymbol{y}^i}{\partial b} \right\} = \sum_{\substack{j=1 \\ j \neq i}}^{r} \frac{-\{\boldsymbol{y}^j\}^T([\partial \boldsymbol{K}/\partial b] - \varsigma^i[\partial \boldsymbol{M}/\partial b])\{\boldsymbol{y}^i\}}{\varsigma^j - \varsigma^i} \{\boldsymbol{y}^j\}$$

$$- \frac{1}{2}\left(\{\boldsymbol{y}^i\}^T \left[\frac{\partial \boldsymbol{M}}{\partial b} \right] \{\boldsymbol{y}^i\} \right) \{\boldsymbol{y}^i\} \tag{15}$$

where r is the number of modes used to approximate the eigenvector sensitivity. Therefore, in order to obtain the loss factor sensitivity it is necessary to solve one eigenvalue problem, one eigenvalue sensitivity analysis, and one eigenvector sensitivity analysis.

To validate numerically the proposed design sensitivity analysis procedure, a clamped-free unconstrained beam problem, identical to the example in the preceding section, is introduced. The length of the damping layer b_1 is selected as the design variable. Table 3 shows

Table 1 Material properties of the beam problem

		LD-400[a]					
Property	Aluminum	a_0	a_1	c_1	d_1	β	T_0, °C
E, MPa	69,000	338.2	2,485.0	0.12	12,222	0.47	15.6
η	0.001	338.2	2,485.0	0.12	12,222	0.47	15.6
ρ, kg/m^3	2,760			1,524			

[a]Material property from Ref. 3.

Table 3 Design sensitivities of the loss factor for the first mode compared with those from the finite difference method (FDM) with 0.1% perturbation ($H_2 = 0.889$ mm)

			Design sensitivity		
No.	ℓ, m	η	Proposed method, $\dot{\eta}$	FDM, $\delta\eta$	$\frac{\dot{\eta}}{\delta\eta} \times 100$, %
1	0.10	6.365E−02	4.505E−01	4.498E−01	100.2
2	0.20	9.163E−02	1.329E−01	1.329E−01	100.0
3	0.30	9.682E−02	2.703E−03	2.527E−03	107.0

Table 2 Comparisons of eigenvalues and loss factors

	Mode 1		Mode 2		Mode 3	
Model	f, Hz	η	f, Hz	η	f, Hz	η
Equivalent beam model	11.01	9.163E−2	65.66	5.424E−2	185.3	4.894E−2
NASTRAN[a]	10.97	9.035E−2	65.08	5.114E−2	183.1	4.620E−2
Ratio, %	100.3	101.1	100.9	106.1	101.2	105.9

[a]The results from linear eigenvalue analysis with the same material constant at each mode frequency of the equivalent beam model.

the calculated design sensitivities for the first mode. The numerical implementations were carried out correctly, and Table 3 proves the validity of the proposed design sensitivity formulation.

IV. Optimization of the Damping Layer Layout

Assuming a uniformly coated damping layer for practical considerations, the optimal design problem of the unconstrained damping layout on beams can be defined as follows:

Find the design variables $\boldsymbol{b}$ such that the following holds.

Maximize:

$$\eta(\boldsymbol{b};\ f, T)$$

Subject to:

$$\text{volume}(\boldsymbol{b}) = \text{constant}$$

$$\boldsymbol{b}_L \leq \boldsymbol{b} \leq \boldsymbol{b}_U \tag{16}$$

where $\boldsymbol{b}_L$ and $\boldsymbol{b}_U$ are the lower and upper bounds of the design variables. Here, an equality constraint is introduced in order to represent the constant volume condition of the damping material during optimization iterations. In this research, a quasi-Newton algorithm is used to solve the optimization problem. The gradient data regarding both the objective and the constraint functions are computed using the analytical sensitivity formula proposed in the preceding section, and are plugged into the optimizer as a user function.

Optimal lengths of an unconstrained damping layer that gives a maximum loss factor for the first mode are determined. As in the preceding section, LD-400 and aluminum are again used. The dimensions of the base beam are fixed, as shown in Fig. 1. Here, the resonant frequency of the first mode is not constant; it shifts a great deal according to the damping layout and temperature. The optimal damping layouts are determined for the clamped–free and clamped–pinned boundary conditions. When selecting the design variables, the mode shapes are considered so that the strain energy stored in the damping material can be dissipated as much as possible. For the clamped-free example, the design variable is only b_1 because the strain energy density decreases monotonically from the clamped side.

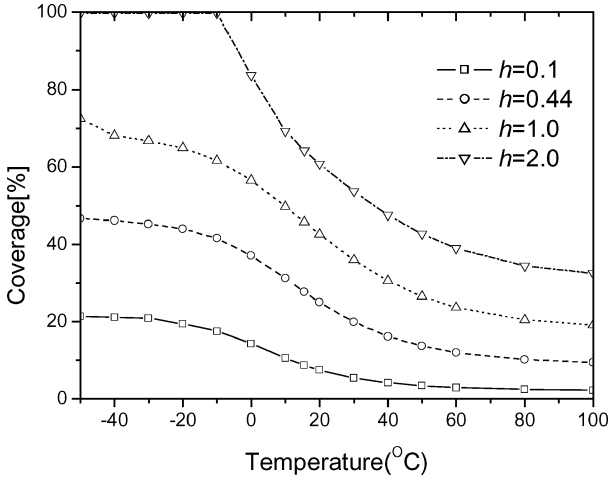

a) Optimum coverage

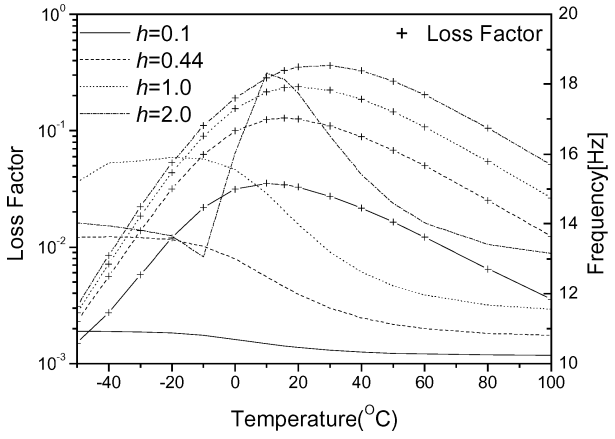

b) Loss factor and eigenfrequency

Fig. 2 Optimum damping layout for the clamped–free boundary condition.

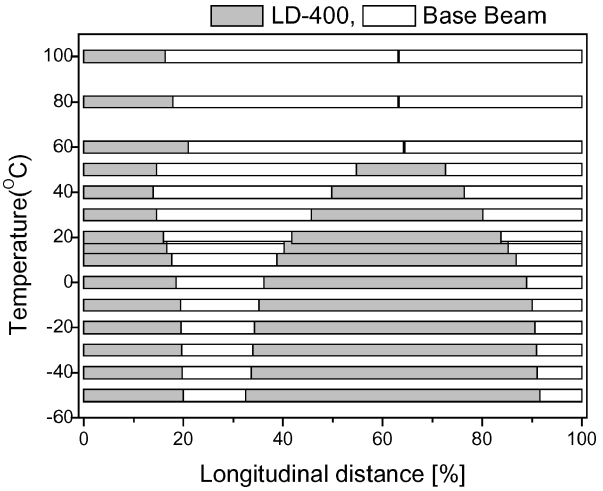

Fig. 3 Overhead view of optimum damping layout for the clamped–pinned boundary condition ($h = 1.0$).

Figures 2 and 3 show the optimal damping layouts for each boundary condition. In the figures, the thickness ratio h corresponds to an initial thickness ratio when the coverage is 50%. These two figures show that the optimum layout is heavily dependent upon the temperature. For a given amount of damping material, the optimum coverage gets smaller, and the optimum height of the damping layer gets thicker in accordance with the increase of temperature. Furthermore, the smaller the given amount of damping material is, the greater is the concentration of the damping material on the high strain energy part, which is the clamped side in the clamped-free example. This occurs in proportion to the rising temperature, and the maximum loss factor for a given amount of damping material is obtained.

V. Conclusions

The optimal damping treatment layouts that give the maximum loss factor on unconstrained beams are identified according to environmental temperatures and thickness ratios. To represent the complex modulus and the loss factor of the viscoelastic layer on beams with respect to frequency and temperature, the four-parameter fractional derivative model is used with the frequency-temperature superposition principle. The equivalent stiffness of the unconstrained beam is calculated using the RUK formula. A finite beam element for the unconstrained beam has been developed and used to solve the nonlinear eigenvalue problem. The analytic design sensitivity formula of the loss factor is derived in order to optimize the layout of the unconstrained damping layer. Numerical examples show that the proposed optimization procedure is very robust for real material.

Acknowledgment

This work was supported by Grant R05-2002-000-00475-0 from the Basic Research Program of the Korea Science and Engineering Foundation.

References

[1]Lifshitz, J. M., and Leibowitz, M., "Optimal Sandwich Beam Design for Maximum Viscoelastic Damping," *International Journal of Solids Structures*, Vol. 23, No. 7, 1987, pp. 1027–1034.

[2]Lumsdaine, A., and Scott, R. A., "Shape Optimization of Unconstrained Viscoelastic Layers Using Continuum Finite Elements," *Journal of Sound and Vibration*, Vol. 216, No. 1, 1998, pp. 29–52.

[3]Jones, D. I. G., *Handbook of Viscoelastic Vibration Damping*, Wiley, New York, 2001, pp. 51–267.

[4]Eldred, L. B., Baker, W. P., and Palazotto, A. N., "Kelvin–Voigt vs Fractional Derivative Model as Constitutive Relations for Viscoelastic Material," *AIAA Journal*, Vol. 33, No. 3, 1995, pp. 547–550.

[5]Sun, C. T., and Lu, Y. P., *Vibration Damping of Structural Elements*, Prentice–Hall, Upper Saddle River, NJ, 1995, pp. 210–238.

[6]Haug, E. J., Choi, K. K., and Komkov, V., *Design Sensitivity Analysis of Structural Systems*, Academic Press, London, 1986, pp. 49–70.

[7]Wang, S. M., and Choi, K. K., "Continuum Sizing Design Sensitivity Analysis of Eigenvectors Using Ritz Vectors," *Journal of Aircraft*, Vol. 31, No. 2, 1993, pp. 457–459.

B. Balachandran
Associate Editor

Flowfield and Aerodynamic Performance of a Turbine Stator Cascade with Bowed Blades

Chunqing Tan*
Chinese Academy of Sciences, 100080 Beijing, People's Republic of China
Atsumasa Yamamoto†
Japan Aerospace Exploration Agency, Tokyo 182-8522, Japan
Haisheng Chen‡
Chinese Academy of Sciences, 100080 Beijing, People's Republic of China
and
Shinpei Mizuki§
Hosei University, Tokyo 184-8584, Japan

Introduction

In turbine stator cascades, the loss near the cascade endwalls contributes to the overall cascade loss significantly.[1] Therefore, it is very important to reduce this. The bowed blade (concept of which was published in the 1960s by Deich et al.[2]) has been considered by numerous researchers as the appropriate blade design to reduce the loss of turbine cascades. An experimental study with bowed stator blade cascade[3] (here referred to as the Wang's cascade) was made and demonstrated that positive bowing could decrease the loss near the endwalls and made the spanwise distribution of the cascade outlet yaw angle uniform. The optimum bowed angle of about 20 deg was found to reduce the cascade loss by up to 40%. However, experiments performed by the present authors on another turbine stator cascade (Yamamoto's cascade) showed that the positive bowing neither reduced the cascade losses near the endwalls nor produced uniform distribution of the outlet yaw flow angle, and no optimum blade bowed angle was found.[4] The different finding from the two experiments is caused mainly by the different cascade setup (with and without the cascade tailgate), the Wang's tailgate extended 5 mm downstream from the blade trailing edge, which can lead to the measured cascade overall loss to include a jet loss at the cascade outlet. Thus, it is important to repeat the detailed experiments using the same Wang's cascade with more extended tailgate.

Experimental Method

The present experiment was conducted with a suction-type low-speed linear cascade wind tunnel at the Japan Aerospace Exploration Agency, Tokyo, Japan. The geometrical and aerodynamic parameters of the cascades presently tested are as follows: blade bowed angles $\varepsilon = 0$, 10, 20, and 30 deg (Fig. 1); blade height $h = 101.0$ mm; blade chord $C = 102.04$ mm; axial blade chord $C_{\text{ax}} = 69.0$ mm; blade pitch $T = 70.5$ mm; cascade outlet angle at the design $\alpha_{\text{out},d} = 19$ deg (from the cascade pitchwise direction); outlet Mach number $M_{\text{out}} = 0.2$; Reynolds number $Re = 4.9 \times 10^5$; freestream turbulence intensity $T_u = 0.5\%$; inlet boundary-layer thickness $\delta_{99} = 24$ mm; and shape factor $\theta = 1.2$. The cascade outlet measurement plane was located at $0.45C_{\text{ax}}$ from the cascade trailing edge. The pitchwise measurement width was 129% of the cascade blade pitch. A five-hole pitot microprobe with head size of 1.5 mm was used to measure the cascade flowfields. The pressure measurement error was estimated at 0.15%. The energy loss coefficient is defined by

$$\xi = \frac{(P_s/P_t)^{(k-1)/k} - (P_s/P_{t,\text{in}})^{(k-1)/k}}{1 - (P_s/P_{t,\text{in}})^{(k-1)/k}} \tag{1}$$

where P_s, P_t, and $P_{t,\text{in}}$ represent local static pressure, local total pressure, and cascade inlet total pressure, respectively, and k ratio of specific heat. A detailed description of the experimental method and analysis method can be found in Ref. 4.

Results and Discussion

Figure 2 shows the energy loss coefficient at the outlet measurement plane. The loss distribution of the straight blade cascade

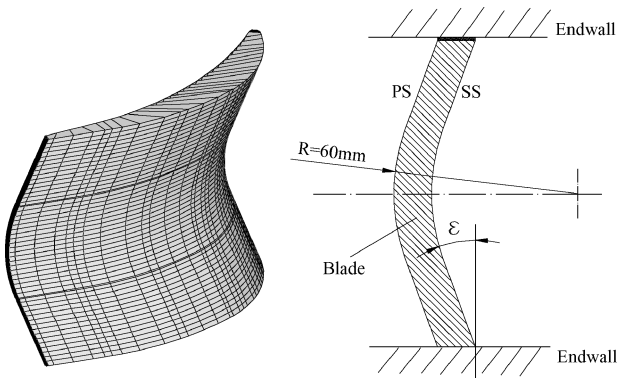

Fig. 1 Three-dimensional view and stacking lines of the bowed blades.

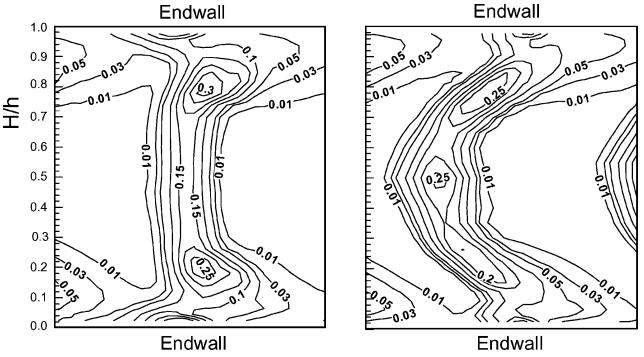

a) $\varepsilon = 0$ deg **b) $\varepsilon = 20$ deg**

Fig. 2 Distributions of the energy loss coefficient at the outlet measurement plane.

Received 7 April 2003; revision received 11 March 2004; accepted for publication 24 June 2004.

*Professor, Institute of Engineering Thermophysics, P.O. Box 2706; tan@mail.etp.ac.cn. Member AIAA.

†Head, Turbomachinery Technology Development Team, Aeroengine Testing Technology Center, 7-44-1 Jindaiji Higashimachi, Chofu-shi; ayamamot@chofu.jaxa.jp.

‡Ph.D. Student, Institute of Engineering Thermophysics, P.O. Box 2706; chen_hs@mail.etp.ac.cn.

§Professor, Department of Mechanical Engineering, 3-7-2 Kajino-cho, Koganei-shi; mizuki@fml.k.hosei.ac.jp.